

Phase space reconstruction in the restricted three-body problem

Marian Gidea*, Frederick Deppe* and Gregory Anderson†

**Department of Mathematics, Northeastern Illinois University, Chicago, IL 60625, U.S.A.*

†Department of Physics and Astronomy, Northeastern Illinois University, Chicago, IL 60625, U.S.A.

Abstract. We study the motion of the infinitesimal mass in the planar circular restricted three-body problem. The infinitesimal mass can undergo regular or chaotic motions. It can be captured by one of the primaries, it can make transfers from one primary to another, or it can even escape those captures. We analyze through statistical methods the time-series given by the time intervals between successive crossings made by the infinitesimal particle to a given Poincaré section. We apply Takens/Yorke embedding theory to reconstruct the phase space from these time series, and we use the correlation dimension of the reconstructed phase space as a tool to distinguish between various types of motions.

Keywords: Three-body problem, phase space reconstruction, correlation dimension.

PACS: 45.50.Pk, 05.45.Pq, 05.45.Tp, 95.10.Ce, 95.10.Fh.

INTRODUCTION

In this paper we propose the application of a phase space reconstruction method to analyze the dynamics in the restricted three-body problem. We use the time series given by the intervals between successive crossings of a given plane of section. We reconstruct the phase space using delay-coordinate vectors formed from this series. We estimate the embedding dimension of the reconstructed phase space as the dimension at which the correlation dimension saturates, as we increase the number of components in the delay coordinate vectors. We use the corresponding correlation dimension of the embedded phase space to detect regular and chaotic trajectories. We also explore, through this method, quasi-periodic, resonant, and resonance transition motions. It is well known that chaotic trajectories can be trapped around a resonance for a long time; this type of behavior was observed in the motion of asteroids and comets (see [1, 15, 20]).

As a first model, we consider the planar circular restricted three-body problem with equal masses. A motivation for this model is the study of binary star systems (see, for example, [4, 5, 6]). The optical observation of such systems is very difficult (see [9]).

To study resonance transitions, we consider a second model represented by the Sun-Jupiter system.

The main advantage of our approach is that it requires little information about the motion of an observable object, namely the successive times when the object assumes a certain angular coordinate with respect to the observer. There is no need of a large number of observations; in our experiments, time series of the order of 10^3 data points provided satisfactory results. Also, this method is computationally cheap and relatively robust. We speculate that due to these advantages, our method could be of use in dynamical astronomy, where information on the motion of celestial bodies is sometimes insufficient. On the other hand, the accuracy of the method can suffer as a consequence of the scarcity of the data; estimates of correlation dimensions are not very accurate if data is not abundant. Error analysis of the numerical computation of the correlation dimension is discussed by Sprott in [18]. Quoting from Sprott: “the literature is devoid of credible calculations of the correlation dimension for most model chaotic systems”. However, in our experiments we do not need an exact computation of the correlation dimension, but we need to verify whether the estimated correlation dimension falls within a certain range of values.

We are not aware of previous attempts of applying phase space reconstruction based on the crossing times of a Poincaré section to the study of the three-body problem. There have been other ways in which time series analysis has been applied to celestial mechanics. Here we will only mention a few of them for comparison. The classical method for detecting chaotic behavior in a dynamical system is that of the Lyapunov exponents. This may take a large amount of computations, particularly if the chaos is weak, and may not provide additional qualitative information, for example, if a regular trajectory is quasi-periodic or resonant. An application of this method to the study of the dynamics of outer-belt asteroids can be found in [14]. The same family of asteroids is studied with the autocorrelation function of

the time series of the osculating elements in [20]. A faster and more sensitive method is the method of twist angles proposed in [2]; this relies on computing the angles between deviations of the orbit and a fixed direction. Tested on the standard map, the method of twist angles was able to differentiate between quasi-periodic and resonant trajectories (see [3]). In [21], a method of time-frequency analysis based on wavelets was applied to the Sun-Jupiter-comet system for values of the Jacobi constant close to Oterma's. This method constructs a frequency map numerically, assigning to each initial condition the computed time-varying frequency $\omega(t)$ of the corresponding trajectory integrated over a fixed time interval. A trajectory with regular motion has a frequency $\omega(t)$ that is constant in time, while a frequency that varies in time suggests a chaotic orbit. Another method for detecting quasi-periodic and chaotic motions, based on the computation of the energy spectrum, is presented in [13].

In contrast with the approach proposed in this paper, all the above methods require a detailed knowledge of the motion over a long period of time. As it is often the case in numerical simulations, it is perhaps better to use the phase-space reconstruction method described in this paper in combination with some other method from the ones mentioned above (if there is sufficient data available), rather than this method alone.

THE RESTRICTED THREE-BODY PROBLEM

The restricted three-body problem refers to the dynamics of two bodies of masses $m_1 \leq m_2$ (referred to as the primaries) that move along circles about their common center of mass, and of a third body, of infinitesimal mass, that is subject to the gravitational attraction of the primaries. The motion of the primaries is not affected by the motion of the infinitesimal mass.

Equations of motion

We will recall the general equations for the planar circular restricted three-body problem. The relative masses of the primaries are $\mu = m_1/(m_1 + m_2)$ and $1 - \mu = m_2/(m_1 + m_2)$. We can choose the units of mass, distance and time so that the gravitational constant is 1, and the period of the circular orbits is 2π . We can study the dynamics relative to a co-rotating system of coordinates (x, y) , for which the positions of the primaries relative to this system are $(-\mu, 0)$ and $(1 - \mu, 0)$ respectively. The motion $(x(t), y(t))$ of the infinitesimal particle relative to the co-rotating frame is described by the second order differential equations:

$$\ddot{x} = 2\dot{y} + \frac{\partial V}{\partial x}, \quad (1)$$

$$\ddot{y} = -2\dot{x} + \frac{\partial V}{\partial y}, \quad (2)$$

$$(3)$$

where V (the effective potential) is given by

$$V(x, y) = \frac{1}{2}(x^2 + y^2) + \frac{1 - \mu}{r_1} + \frac{\mu}{r_2}, \quad (4)$$

with $r_1 = ((x + \mu)^2 + y^2)^{1/2}$ and $r_2 = ((x - 1 + \mu)^2 + y^2)^{1/2}$ representing the distances from the infinitesimal mass to the primaries. See [17]. The phase space of the system is 4-dimensional. The energy function

$$H(x, y, \dot{x}, \dot{y}) = \frac{1}{2}(\dot{x}^2 + \dot{y}^2) - V(x, y), \quad (5)$$

is a first integral of the system. An equivalent first integral is the Jacobi integral $C(x, y, \dot{x}, \dot{y}) = -2H(x, y, \dot{x}, \dot{y})$. The energy manifold

$$\{(x, y, \dot{x}, \dot{y}) \mid H(x, y, \dot{x}, \dot{y}) = \text{constant}\} \quad (6)$$

is 3-dimensional, and its projection onto the configuration space (x, y) is called a Hill's region. Its boundary is a zero velocity surface. The topology of Hill's regions depends on the energy level. Each trajectory is confined to the Hill's region for the corresponding energy level. See Figure 1.

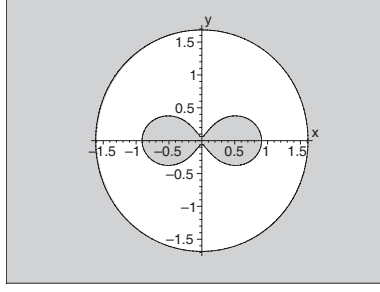


FIGURE 1. Hill's region corresponding to an energy level slightly below that of L_1 , for $\mu = 1/2$.

There are five equilibrium points for this problem. Three of them are collinear with the primaries, and each of the other two forms an equilateral triangles with them. In this paper, we are only interested in the equilibrium point L_1 between the primaries. The distance from L_1 to the less massive primary is given by the only positive solution to Euler's quintic equation (see [17]):

$$\gamma^5 - (3 - \mu)\gamma^4 + (3 - 2\mu)\gamma^3 - \mu\gamma^2 + 2\mu\gamma - \mu = 0.$$

For the case when the primaries have equal masses, we have $\mu = 0.5$, hence $\gamma = 0.5$, so L_1 is at $x_{L_1} = 0$. For the Sun-Jupiter system, we have $\mu = 0.0009573$, hence $\gamma = 0.0667583$, so L_1 is at $x_{L_1} = 0.0658010$.

To study chaotic transfers, we will consider an energy level slightly below that of L_1 . The corresponding Hill region consists of two lobes, one lying in $x < 0$ and the other one in $x > 0$, which are connected through a narrow dynamical channel. The dynamics near L_1 is of saddle-center type. There exist periodic orbits (Lyapunov orbits) near L_1 , located inside the dynamical channel. These Lyapunov orbits possess stable and unstable manifolds that intersect each other at points away from L_1 . The infinitesimal particle will typically move inside one lobe or another of the Hill region, and transfer between $x < 0$ and $x > 0$, through the dynamical channel, in a chaotic fashion.

Poincaré sections

One way to investigate the dynamics in the circular restricted three-body problem is by discretizing the system through the Poincaré first return map associated to some Poincaré section. For example, we can define a Poincaré section $\Sigma_1 = \{(x, y, \dot{x}, \dot{y}) \mid x = 1 - \mu, y > 0, \dot{x} > 0\}$ or $\Sigma_2 = \{(x, y, \dot{x}, \dot{y}) \mid x = x_{L_1}, y > 0, \dot{x} > 0\}$. In the planar circular case the total energy is preserved along the motion, so each trajectory $(x(t), y(t), \dot{x}(t), \dot{y}(t))$ lies on a fixed energy manifold. The intersection of a trajectory with the Poincaré section Σ_1 or Σ_2 yields a fixed value for the x -coordinate, and from the energy condition we can solve for \dot{x} with respect to y and \dot{y} . Thus, the intersections of a trajectory $(x(t), y(t), \dot{x}(t), \dot{y}(t))$ with a Poincaré section as above is given by the coordinates (y, \dot{y}) corresponding to the intersection point; each such (y, \dot{y}) uniquely determines the whole orbit.

The dynamics of the Poincaré map shows two basic types of motions: regular motions confined to elliptic islands, and chaotic motions scattered around these islands. See Figure 2. In the center of each elliptic island there is a point corresponding to exactly one periodic, stable, resonant orbit. A trajectory that is initialized on one of the closed curves that is a part of an elliptic island will remain on the same curve, provided the center of the island is a fixed point for the Poincaré map, or it will jump from one closed curve, part of an elliptic island, to another curve, part of another elliptic island, in a periodic fashion, provided that the center of the island is a periodic point for the Poincaré map. In the 3-dimensional energy manifold, these closed curves correspond to invariant 2-dimensional tori. The motion on such a torus can be quasi-periodic, in which case it will fill up a region dense in the surface of the torus, or resonant, in which case it will lie on a 1-dimensional torus. If $\omega = (\omega_1, \omega_2)$ is the frequency vector of the motion on the torus, then a quasi-periodic motion is characterized by a condition $k_1\omega_1 + k_2\omega_2 \neq 0$ for all integers k_1, k_2 , while a resonant motion is characterized by a condition $k_1\omega_1 + k_2\omega_2 = 0$ for some integers k_1, k_2 .

The existence of chaotic motions has been one of the key arguments in proving the non-integrability of the three-body problem. One way to argue rigorously the existence of chaotic motion is by showing the existence of transverse homoclinic connections to Lyapunov orbits near L_1 . This has been proved analytically in the case $\mu \simeq 0$ (see, for example [12]), and numerically (see, for example [7]). Then Birkhoff-Smale Homoclinic Orbit Theorem implies the

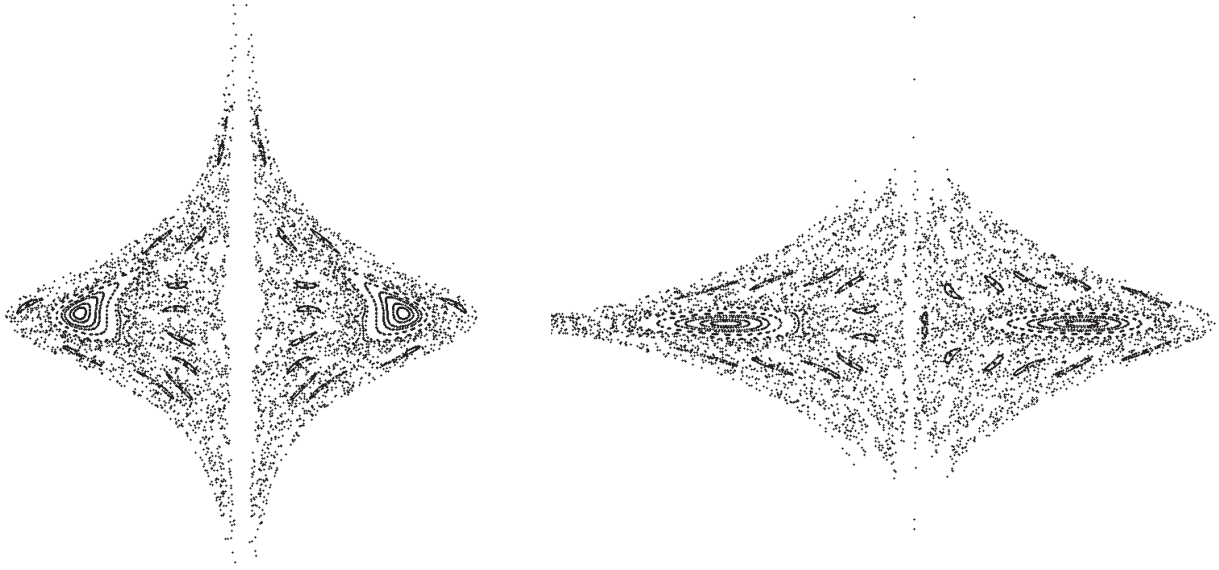


FIGURE 2. Poincaré sections in the planar circular restricted three-body problem corresponding to a Jacobi constant $C = 3.95$, for $\mu = 0.5$. Left – in (y, \dot{y}) -coordinates, corresponding to $x = 0.5$; right – in (x, \dot{x}) -coordinates, corresponding to $y = 0$. The small elliptic islands in the plot surround a periodic orbit of period 12 for the Poincaré map.

existence of a subsystem that possesses symbolic dynamics. However, this argument identifies only a measure zero set of chaotic trajectories. Nevertheless, numerical studies suggest that the phase space contains a full measure set of chaotic trajectories.

PHASE SPACE RECONSTRUCTION AND CORRELATION DIMENSION

In this section we review briefly the method of phase space reconstruction based on delay coordinate vectors. Precise formulations of the statements presented below have been provided by Takens [19], and Sauer, Yorke and Casdagli [16]; a good introduction to the subject is given by Huke [10].

Suppose that $f : M \rightarrow M$ is a discrete dynamical system, where M is a compact, m -dimensional, C^r -differentiable manifold ($r \geq 2$), and f is a C^r -diffeomorphism. Let $h : M \rightarrow \mathbb{R}$ be a C^r -differentiable function, which plays the role of a measurement of some physical quantity for the orbits of f . To each finite orbit $\{x, f(x), \dots, f^N(x)\}$ of a point $x \in M$, where $N > 0$ is fixed, we can associate the time series $\{h(f^i(x))\}_{i=1, \dots, N}$. Let $\Phi : M \rightarrow \mathbb{R}^N$ be the mapping given by

$$\Phi(x) = (h(x), h(f(x)), \dots, h(f^N(x))).$$

Takens's Theorem states that for C^r -generic maps f and h , the mapping Φ is an embedding of M in \mathbb{R}^N provided $N \geq 2m + 1$. Moreover, there is a natural dynamics on $\Phi(M)$, induced by the left shift map $\bar{f} : \Phi(M) \rightarrow \Phi(M)$ given by:

$$\bar{f}(h(x), h(f(x)), \dots, h(f^N(x))) = (h(f(x)), \dots, h(f^{N+1}(x))).$$

The map Φ is a conjugacy between the dynamics on M and the dynamics on $\Phi(M)$; that is, $\Phi \circ f = \bar{f} \circ \Phi$, with Φ continuous and surjective. In summary, the map Φ not only provides us with a copy of M in \mathbb{R}^N , but also with a copy of the dynamics on M induced by f . In particular, the periodic orbits of f are mapped into periodic orbits of \bar{f} , and dense orbits for f are mapped into dense orbits for \bar{f} . The same method can be used to reconstruct an attractor $A \subset M$ for f from a time series associated to an orbit dense in A . It is sufficient to choose a dimension N of the embedding space bigger than $2d + 1$, where d is the box-counting dimension (fractal dimension) of A .

In practice, this method is applied as follows. We have a dynamical system $f : M \rightarrow M$ that we would like to analyze. Beginning with some initial state, the evolution of the system results in a succession of states described by a finite orbit $\{x, f(x), \dots, f^n(x)\}$ of a point $x \in M$. Usually we cannot obtain complete information on the states of the system, but we can measure some quantity associated to each state; this is performed through a measurement function $h : M \rightarrow \mathbb{R}$. The measurement function defines a finite time series $\{x_i\}_{i=0, \dots, n}$ given by $x_i = h(f^i(x))$. Assuming that

the orbit $\{x, f(x), \dots, f^n(x)\}$ is dense in some invariant set S of f , we want to reconstruct the set S and the dynamics of f on S from this time series. We consider the delay coordinate vectors

$$v_i = (x_i, x_{i+1}, \dots, x_{i+(d-1)}),$$

where d (the dimension of the phase space) is a positive integer, and $i \geq 0$. We denote this set of vectors by \bar{S} . On \bar{S} we consider the map \bar{f} given by

$$\bar{f}(x_i, x_{i+1}, \dots, x_{i+(d-1)}) = (x_{i+1}, x_{i+2}, \dots, x_{i+d}).$$

The set of vectors \bar{S} together with the map \bar{f} constitutes a model for the dynamics of f on S . In order for this model to be accurate, we need the dimension d of the reconstructed phase space to be sufficiently large; otherwise the model may exhibit some tangles or self-crossings that are not present in the original system S . Although we do not have an a priori knowledge of the box-counting dimension of S , we can still find the correct embedding dimension through the following procedure. We gradually increase the dimension d of the delay coordinate vectors and compute the box dimension of the reconstructed set for each d . In general, the computed box-counting dimension will be an increasing function of d . Beginning with some value $d = d_e$, the box-counting dimension will stabilize; this value d_e is the smallest dimension for which we obtain an embedding of S in the reconstructed phase space \mathbb{R}^d . At this point we also have that the dynamics of f on S is reproduced accurately by the dynamics of \bar{f} on the reconstructed phase space \bar{S} .

The box-counting dimension of a set is quite expensive to compute numerically. An empirical alternative to it is the correlation dimension. The correlation dimension of the set

$$\bar{S} = \{v_0, v_1, \dots, v_{n-(d-1)}\}$$

can be computed as follows. We first compute the correlation function $C(r)$ which measures the proportion of pairs of points from \bar{S} that are within r units from one another:

$$C(r) = \frac{\#\{(w_1, w_2) \mid w_1, w_2 \in \bar{S} \text{ and } \|w_1 - w_2\| < r\}}{\#\{(w_1, w_2) \mid w_1, w_2 \in \bar{S}\}},$$

where $r > 0$. It turns out that $C(r)$ is proportional to r^d for some fixed $d > 0$ and all sufficiently small r , where d is exactly the correlation dimension of the set \bar{S} .

Then the correlation dimension of \bar{S} is defined as

$$\text{corrdim}(\bar{S}) = \lim_{r \rightarrow 0} \frac{\ln C(r)}{\ln r}, \quad (7)$$

provided that the limit exists. In practice, since the data set in \bar{S} is only finite, one cannot compute the above limit as $r \rightarrow 0$. Moreover, if r is made smaller than the shortest distance between any two distinct points in \bar{S} , then $C(r) = 0$. On the other hand, if r is made larger than the diameter of the set \bar{S} , then $C(r) = 1$. A practical way to estimate the correlation dimension is to plot $\ln C(r)$ versus $\ln r$ and to estimate the slope of the median portion of the plot. The graph will usually flatten out for all sufficiently small values of r , and also for all sufficiently large values of r . The remainder of the graph will contain a part that is almost linear. The least square method is applied to this linear part of the graph. The slope of the resulting linear approximation gives the correlation dimension of \bar{S} . In general, the correlation dimension is smaller than the box counting dimension, but they are usually very close. For details, see [8].

The correlation dimension computed this way is reasonably accurate when the data set is rather big. If there is insufficient data, the correlation dimension can only be used as an indicator of whether or not the invariant set is likely to fill up a region of positive measure in \mathbb{R}^d , for some prescribed $d > 0$.

EXPERIMENTS

We generate numerically trajectories of the three-body problem and we record the times $\{t_i\}_i$ at which the trajectories cross some fixed Poincaré section Σ . From this data we generate the time series $\{\Delta t_i\}_i$ consisting of the time intervals $\Delta t_i = t_{i+1} - t_i$ between successive crossing. We are interested in two problems. The first problem is to use this time series to distinguish between regular and chaotic orbits. The second problem is that, in the case when the infinitesimal mass undergoes transfers between one primary and another, we want to detect whether or not these transfers occur chaotically.

For the first problem we consider trajectories that are evolving within one of the lobes of the Hill region, say about the primary at $x = 1 - \mu$, and we record the times at which these trajectories cross the Poincaré section $\Sigma_1 = \{x = 1 - \mu\}$. It is possible that at some point these trajectories transit to the other lobe; in this case, we continue to record the times of crossing with Σ_1 only after they go back to the original lobe.

For the second problem we consider trajectories that execute transitions from one lobe of the Hill region to the other, and we record the times at which these trajectories cross the Poincaré section $\Sigma_2 = \{x = 0\}$.

In each case, we reconstruct the phase space from the time series $\{\Delta t_i\}_i$. We compute the correlation dimensions for the phase spaces reconstructed in dimensions $d = 1, 2, \dots$, and we find a dimension d from which the correlation dimension stabilizes. We will not seek the minimal embedding dimension d_e , but some dimension d for which the embedding in \mathbb{R}^d is guaranteed. We use the correlation dimension corresponding to the dimension d to distinguish the type of trajectory that we have. To test the validity of our predictions, we compare the results of the time series analysis with the plot of the intersections between the trajectory and the corresponding Poincaré section.

Periodic motions

In our experiments, we found that periodic motions are characterized by correlation dimensions close to 0, within a margin of error of 0.2. This agrees with the theory, since a periodic orbit corresponds to a finite set of points in the Poincaré section, whose dimension is 0.

As an example, we consider a symmetric periodic orbit of initial condition $x = 0, y = 0, \dot{x} = 0.35, \dot{y} = 0$, corresponding to a Jacobi constant approximately equal to $C = 3.8775$, as shown in Figure 3. The winding number of this orbit is 5. This equals the number of points in the Poincaré section.

We will discuss the numerical experiments for this periodic orbit in full details, to illustrate the implementation of the method, and also to serve us as a guide in the sequel. We have generated the time series $\{\Delta t_i\}_i$ of 1280 data points, where $\{t_i\}_i$ are the intersection times with the plane of section Σ_1 . For this data set, the Jacobi constant is preserved up to the 4-th decimal place during integration. We disregard the first 100 data points, to avoid errors due to temporal correlation. Hence, only 1180 terms are used. We first use 2-dimensional coordinate vectors of the type $\{(\Delta t_i, \Delta t_{i-1})\}_i$ to reconstruct the phase space $\bar{S}(2)$ in 2-dimensions. The reconstructed phase-space consists of 5 points; the number of points matches the winding number of the orbit. See Figure 3.

Using the formula (7), we evaluate the correlation integral $C(r)$ for successive values of $r = 2^{-1}, \dots, 2^{-10}$ and we compute directly the corresponding values of the ratio $\log(C(r))/\log(r)$. We obtain

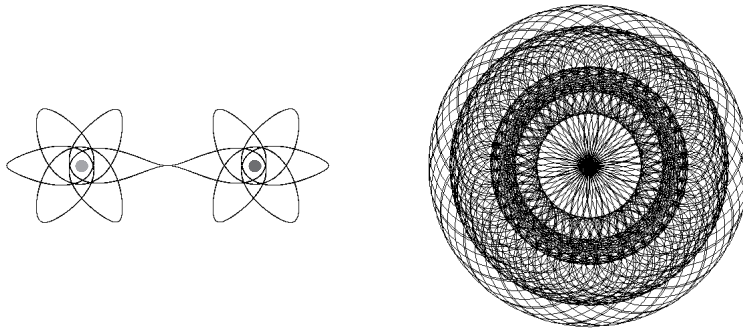
r	2^{-1}	2^{-2}	2^{-3}	2^{-4}	2^{-5}	2^{-6}	2^{-7}	2^{-8}	2^{-9}	2^{-10}
$\log(C(r))/\log(r)$	1.8379	.9189	.7747	.5810	.4648	.3873	.4326	.4570	.4523	.4240

It is not reliable to estimate $\lim_{r \rightarrow 0} (\log(C(r))/\log(r))$ as the tail value of the above sequence. As described in the previous section, a better method is to plot the data $\log(C(r))$ versus $\log(r)$ and to apply the linear regression to the middle portion of this plot.

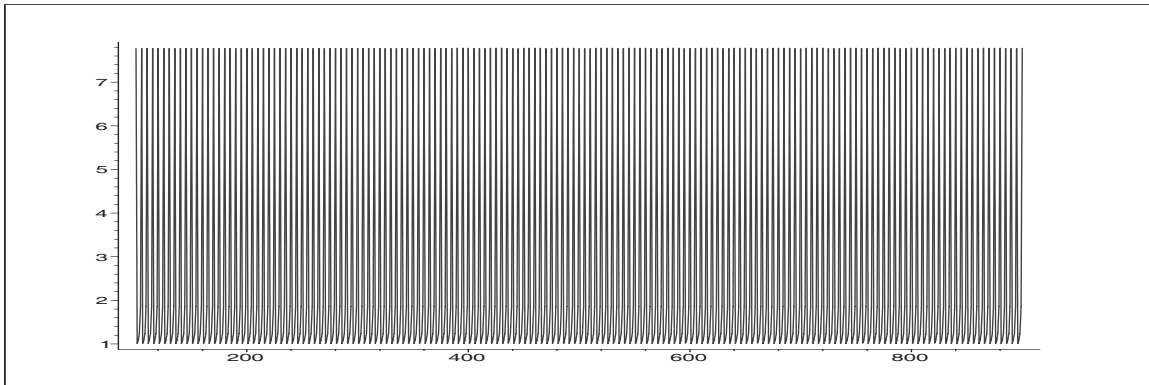
x	-0.6931	-1.3862	-2.0794	-2.7725	-3.4657	-4.1588	-4.8520	-5.5451	-6.2383	-6.9314
y	-1.2739	-1.2739	-1.6111	-1.6111	-1.6111	-1.6111	-2.0990	-2.5345	-2.8222	-2.9390

We identify in the plot the regions at the ends of plot where the graph starts to approach horizontal asymptotes, and we apply linear regression to the remainder of the plot. We identify the linear part of the middle section of the plot by successive trials, enlarging or diminishing the middle range and applying the least square method until the linear approximation stabilizes. See Figure 3. The equation of the linear approximation that we found is $y = -1.6111$. The slope of this line gives us the correlation dimension of the reconstructed phase space, i.e., $\text{cordim}(\bar{S}(2)) = 0$.

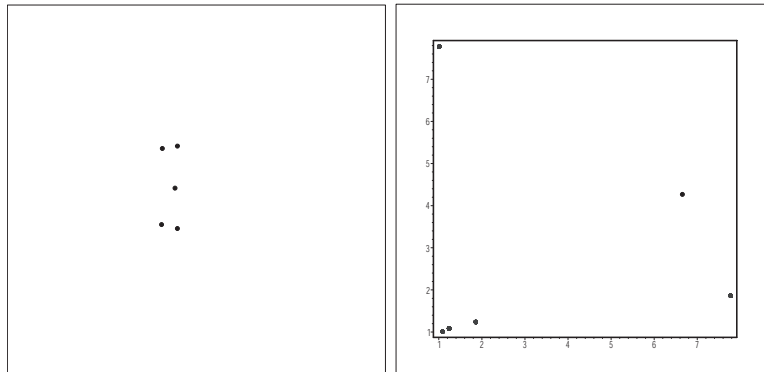
If we repeat the experiment for 1-dimensional delay coordinate vectors $\{\Delta t_i\}_i$, the linear regressions comes out $y = -1.5936 + 0.005x$, so $\text{cordim}(\bar{S}(1)) \approx 0.005$. Although this is quite close to 0, we have a small error since the 1-dimensional phase space reconstruction does not guarantee the elimination of all possible self-crossings. On the other hand, when we repeat the experiment for 3-dimensional delay coordinate vectors $\{(\Delta t_i, \Delta t_{i-1}, \Delta t_{i-2})\}_i$ we find out that $y = -1.6111$ and so $\text{cordim}(\bar{S}(3)) = 0$. Higher dimensional phase space reconstructions confirm that $\text{cordim}(\bar{S}(d)) = 0$, for $d \geq 2$. Thus, we conclude that the correlation dimension for the reconstructed phase space is $\text{cordim}(\bar{S}) = 0$. This remarkably coincides with the theoretical value.



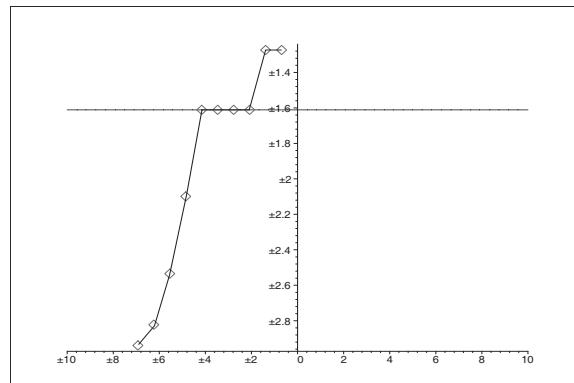
Left – periodic orbit in the co-rotating frame; right – periodic orbit in the inertial frame.



Plot of the $\{\Delta t_i\}_i$ time-series.



Left – Poincaré plot at $x = 1 - \mu$; right – reconstructed phase space in \mathbb{R}^2 .



Correlation dimension and least square approximation.

FIGURE 3. Periodic orbit.

These experiments emphasize the effectiveness of using linear regression to estimate $\lim_{r \rightarrow 0} (\log(C(r))/\log(r))$ as opposed to successive approximations. Also, we learn that the theoretically lowest possible embedding dimension does not guarantee a good numerical estimate on the correlation dimension of the reconstructed phase space. However, finding the optimal embedding dimension is beyond the scope of this paper.

Quasi-periodic motions

In our experiments, we found that quasi-periodic orbits are characterized by a correlation dimension close to 1. This is in agreement with the theory: a quasi-periodic orbit will fill up a 2-dimensional torus, whose intersection with a Poincaré section will be a 1-dimensional curve. We tolerate a range of values of ± 0.2 about 1.

As an example, we consider a quasi-periodic orbit of initial conditions $x = 0.5, y = -0.28, \dot{x} = 0.9554017961, \dot{y} = 0$, corresponding to the Jacobi constant $C = 3.95$. We have generated the time series $\{\Delta t_i\}_i$ of 700 data points, where $\{t_i\}_i$ are the intersection times with the plane of section Σ_1 . For this data set, the Jacobi constant is preserved up to the 4-th decimal place during integration. The orbit and the corresponding time series are shown in Figure 4. The Poincaré plot and reconstructed phase space in 2- and 3-dimensions are also shown in Figure 4. When we compute the correlations dimension, we find that $\text{cordim}(\bar{S}) \approx 1.08$ and it stabilizes beginning a dimension $d = 3$; see Figure 4.

There are some technical problems when too many data points are numerically generated for a quasi-periodic orbit. Such an orbit is usually unstable, and the accumulation of error during integration will result in many points leaving the corresponding torus and ending up in the chaotic sea or on other elliptic islands. The reconstructed phase space will show a closed curve and scattered points around it. These extra points will affect the computation of the correlation dimension. To fix the problem, the time series should be restricted to its quasi-periodic regime.

Resonant motions

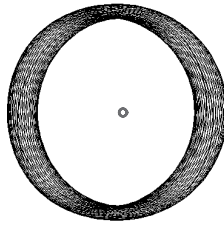
In our experiments, we found that resonant orbits are characterized by a correlation dimension greater than but close to 0. This is in agreement with the theory: a resonant orbit will fill up a 1-dimensional torus (closed curve) lying on the surface of some 2-dimensional torus. The 1-dimensional torus will cut the Poincaré section in a finite set of points. However, resonant orbits are quite unstable; in practice, one will usually see only orbits close to resonance. In this case, the Poincaré plot will consist in clusters of points accumulated around a finite number of locations. The farther the motion is from a resonance, the more spread out those clusters are, and the closer to 1 the correlation dimension is. We will not provide a range of values for the correlation dimensions that is associated to resonant motions; such a range would unavoidably be artificial. In our experiments, we found trajectories that follow a resonant regime for about 1000 revolutions about the mass and whose correlation dimension is between 0.2 and 0.5.

As an example, we consider a resonant orbit of initial conditions $x = 0.3, y = 0, u = 0, v = -0.08$, corresponding to the Jacobi constant $C = 6.3336$. This orbit is in a resonance of 22 : 1 with respect to the motion of the nearby primary. We have generated the time series $\{\Delta t_i\}_i$ of 2000 data points, where $\{t_i\}_i$ are the intersection times with the plane of section Σ_1 . For this data set, the Jacobi constant is preserved up to the 4-th decimal place during integration. The orbit, the corresponding time series, the Poincaré plot and reconstructed phase space in 2- and 3-dimensions are shown in Figure 5. For the correlations dimension, we found that $\text{cordim}(\bar{S}) \approx 0.3$ and it stabilizes beginning a dimension $d = 4$; see Figure 4.

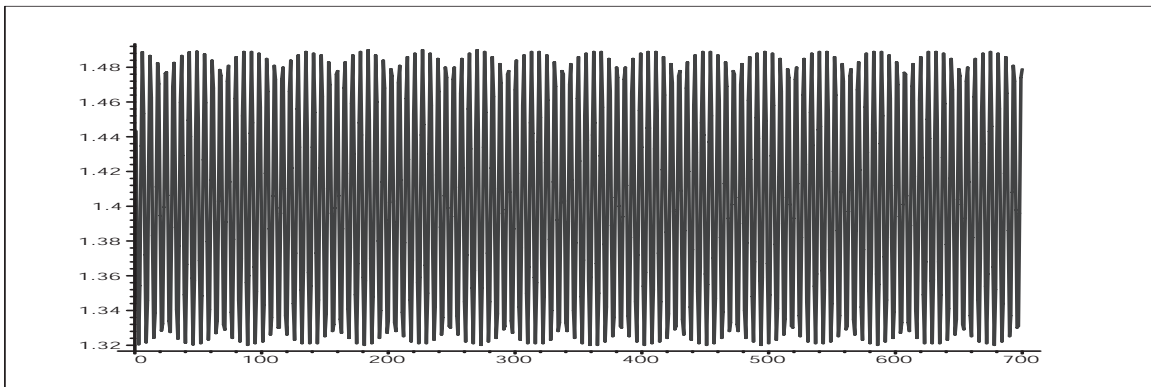
Chaotic motions

In our experiments, we found that chaotic orbits are characterized by a correlation dimension less than but close to 2. This is in agreement with the theory: a resonant orbit will fill up a 2-dimensional region corresponding to the chaotic sea in the Poincaré section. Empirically, we will tolerate a range of values of ± 0.2 about 2.

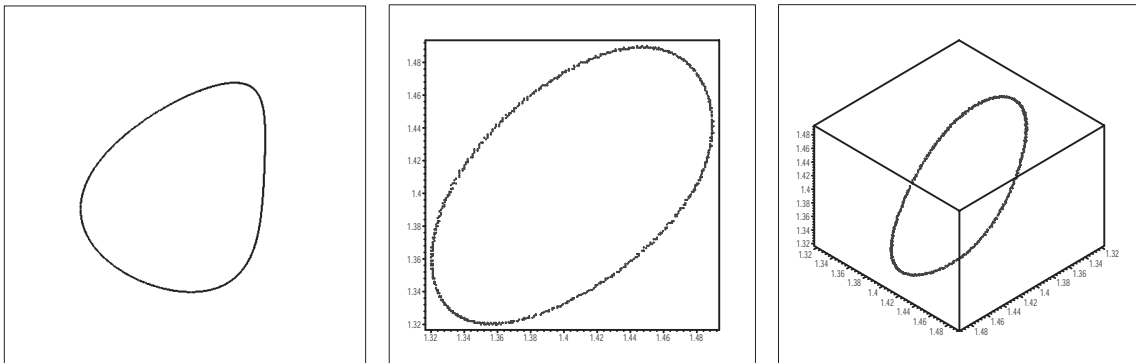
As an example, we consider a chaotic orbit corresponding to $C = 3.95$. We have generated the (y, \dot{y}) -coordinate Poincaré plots corresponding to the sections $x = 0.5$ and $x = 0$; they are shown in Figure 6. The plot corresponding to $x = 0.5$ reveals a richer structure than the one corresponding to $x = 0$. We are interested to classify the transfers of the infinitesimal mass between $x > 0$ and $x < 0$; therefore, we use the time series corresponding to $x = 0$ to reconstruct the phase space. We have generated a time series $\{\Delta t_i\}_i$ of 1400 data points; the Jacobi constant is preserved up to the 4-th



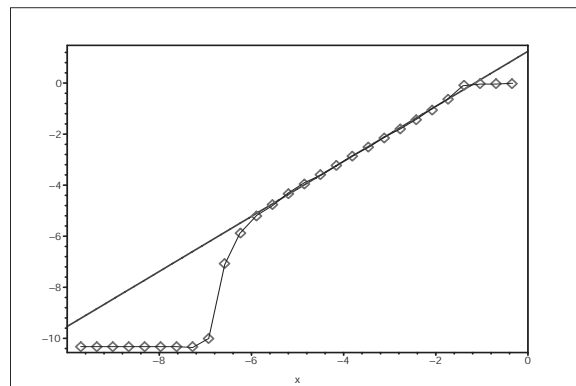
Quasi-periodic orbit around a primary, in a co-rotating frame.



Plot of the $\{\Delta t_i\}_i$ time-series for a quasi-periodic motion.

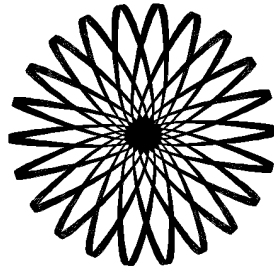


Left – Poincaré plot at $x = 1 - \mu$; middle – reconstructed phase space in \mathbb{R}^2 ; right – reconstructed phase space in \mathbb{R}^3 .

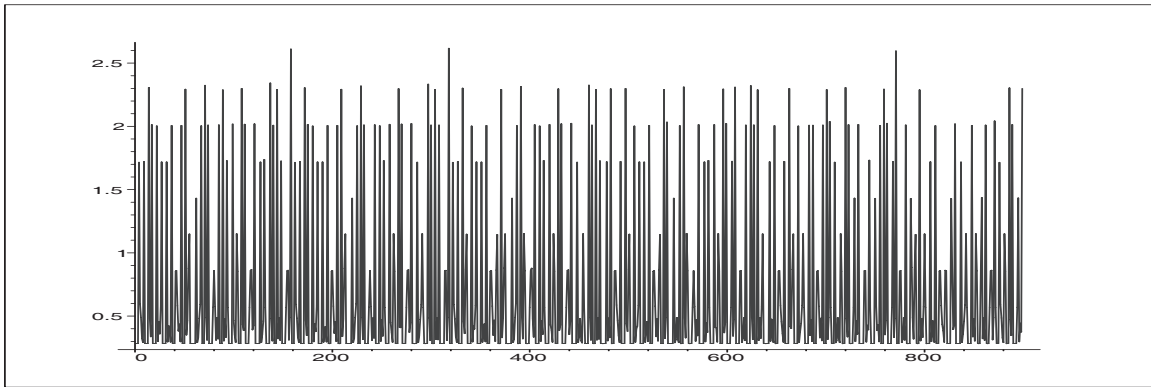


Correlation dimension and least square approximation.

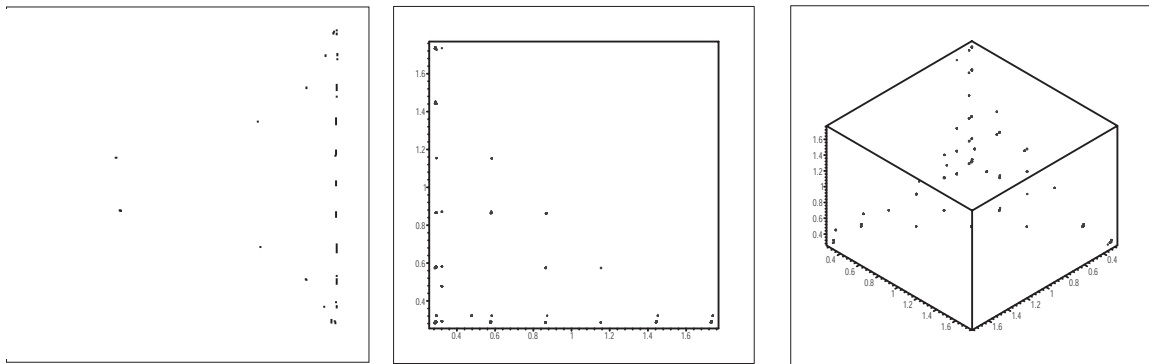
FIGURE 4. Quasi-periodic orbit



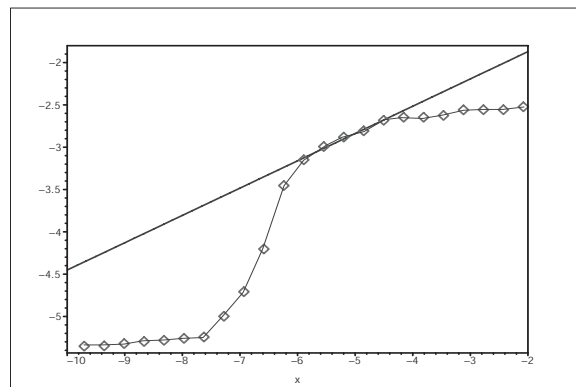
Resonant orbit about a primary, in a co-rotating frame.



Plot of the $\{\Delta t_i\}_i$ time-series.

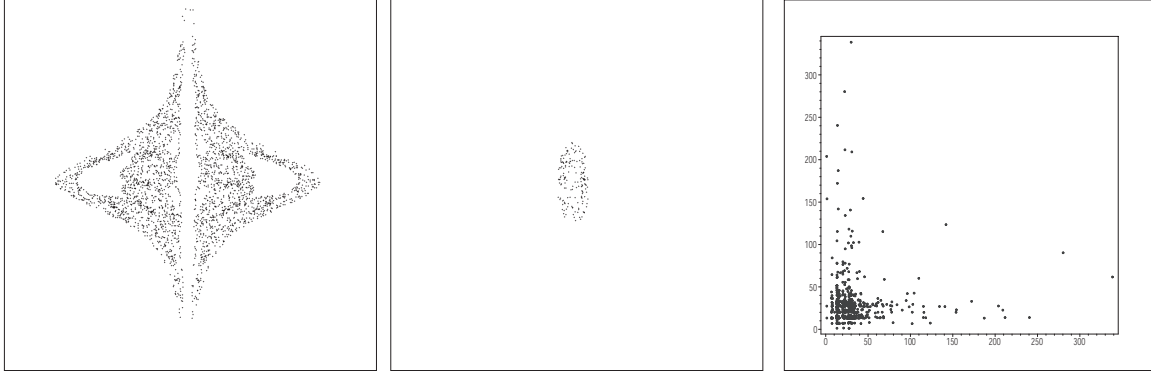


Left – Poincaré plot at $x = 1 - \mu$; middle – reconstructed phase space in \mathbb{R}^2 ; right – reconstructed phase space in \mathbb{R}^3 .

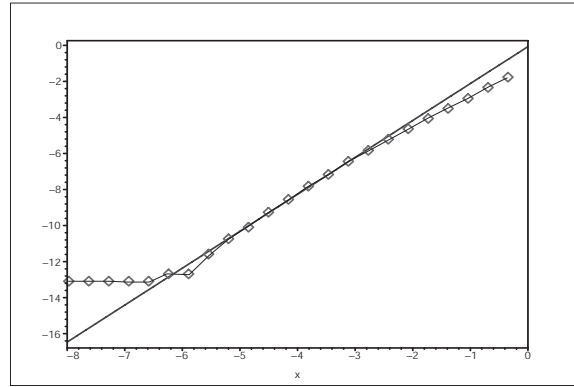


Correlation dimension and least square approximation.

FIGURE 5. Resonant orbit, of 22 : 1 resonance.



Left – Poincaré plot at $x = 0.5$; middle – Poincaré plot at $x = 0$; right – reconstructed phase space in \mathbb{R}^2 .



Correlation dimension and least square approximation.

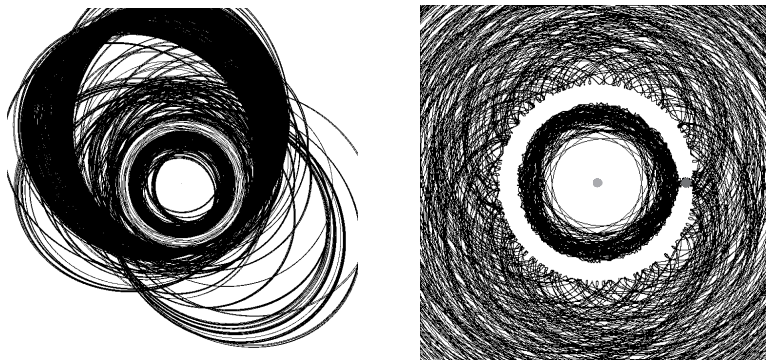
FIGURE 6. Chaotic transfers between primaries.

decimal place during integration. The reconstructed phase space in \mathbb{R}^2 is shown in Figure 6; it looks like a scattered set of points. For the correlations dimension, we found that $\text{cordim}(\bar{S}) \approx 2.0$ and it stabilizes beginning dimension $d = 4$; see Figure 6. This agrees with our expected range of values for the correlation dimension, which characterizes chaotic motions.

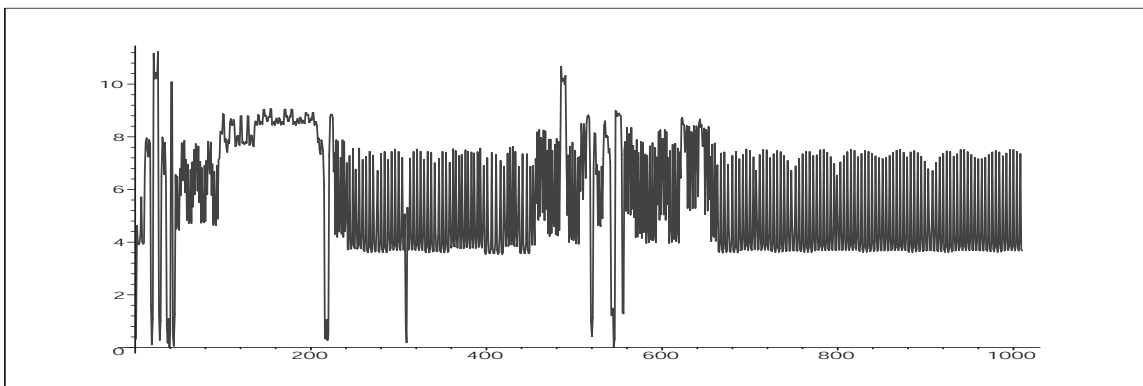
Resonance trapping

An example of resonance trapping is provided by the dynamics of Jupiter's comet Oterma. We model Oterma's dynamics as a planar circular restricted three-body problem, where the primaries correspond to Jupiter and the Sun, and the mass ratio is $\mu = 0.0009537$. This comet makes rapid transitions back and forth between heliocentric orbits outside the orbit of Jupiter and heliocentric orbits inside the orbit of Jupiter. The interior heliocentric orbit is close to a $3 : 2$ resonance, while the exterior heliocentric orbit is close to a $2 : 3$ resonance. In the Poincaré section corresponding to $x = 1 - \mu$, these orbits correspond to resonance islands (see Figure 7). The trajectory is temporarily trapped by one resonant island, where the dynamics is almost regular, then is released and is eventually captured by the other resonant island, while it can visit some other resonant island in between, such as a $1 : 2$ resonance. The Jacobi constant corresponding to the orbit of Oterma is approximately $C = 3.03$.

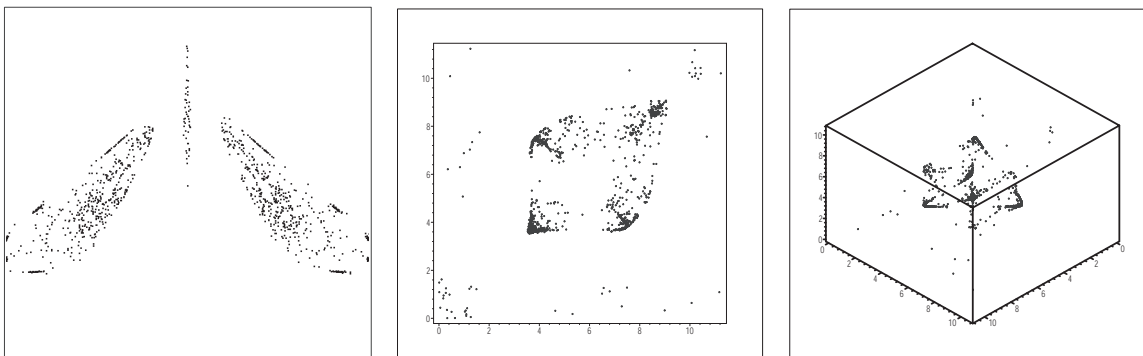
As an example of possible dynamics for Oterma, we started with the initial conditions $x_0 = 0.88, y_0 = 0, \dot{x}_0 = 0.092, \dot{y}_0 = 0.14163$. For the time series, we use the Poincaré section $\Sigma_3 := \{(x, y, \dot{x}, \dot{y}) \mid y = 0, x < -\mu, \dot{y} > 0\}$. However, in Figure 7 we show the Poincaré section corresponding to Σ_1 , since it seems to provide a better evidence of the resonant islands: they look like the wings and the body of the mosquito. We have generated a time series of 1000 points. We estimated the correlation dimension of the reconstructed phase space being $\text{cordim}(\bar{S}) = 1.8$, saturating in dimension 4. See Figure 7. This agrees with our expectations that an orbit that is successively captured by resonances



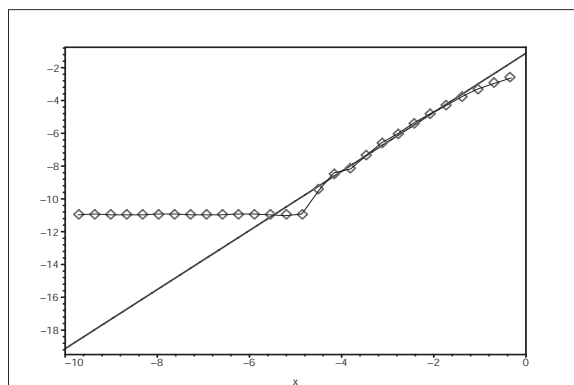
Left – orbit in an inertial frame; right – orbit in a co-rotating frame.



Plot of the $\{\Delta t_i\}_i$ time-series.



Left – Poincaré plot at $x = 1 - \mu$; middle – reconstructed phase space in \mathbb{R}^2 ; right – reconstructed phase space in \mathbb{R}^3 .



Correlation dimension and least square approximation.

FIGURE 7. Resonance trapping.

and wander chaotically from one resonance to another will have a correlation dimension larger than 1 – corresponding to the resonances – and less than 2 – corresponding to chaotic transfers.

FINAL REMARKS AND CONCLUSIONS

We performed the numerical computation of the trajectories with the program Dynamic Solver (author Juan M. Aguirregabiria). We used the integrator Dormand-Prince 8(5,3) with variable step-size. This is not a symplectic integrator; the energy is not conserved during integration. To compensate for this, we restricted the size of the data collected so that the variations in the energy are kept reasonably small. Since the accuracy in computing the correlation dimension is low anyway, we opted for a margin of error in the Jacobi constant $\Delta C \leq 10^{-4}$. It is worth noting that the variation of the Jacobi constant during numerical integration depends on type of the orbit that are generated: stable orbits result in smaller ΔC in the long run when compared to irregular or chaotic orbits. The code for computing the correlation dimension was written in Maple.

The correlation dimension is just one way to measure the fractal dimension of a reconstructed set. It is perhaps the simplest way to formulate theoretically, but it is somewhat subjective and does not indicate the penalty paid for too low an embedding dimension. A more accurate and less computationally intensive procedure is the method of ‘false nearest neighbors’, which identifies the number of points that appear to be the nearest neighbors because the dimension of the reconstructed phase space is too small. When the number of false nearest neighbors drops to zero, it means that self-crossings were eliminated and the proper embedding dimension has been reached. See [11].

The conclusion of these investigations is that, given a time-series consisting in the crossing times of some Poincaré sections, by using phase space reconstruction techniques we can distinguish reasonably well between regular and chaotic motions, and between regular and chaotic transfers, even though the observed data is neither very large nor very accurate. The shortcomings of the method are that the correlation dimension estimator is not very precise, and it leaves ‘gray’ ranges of values for which the type of trajectories cannot be properly determined. In the future, we hope to be able to improve the methods outlined in this paper by using other estimators such as the ‘false nearest neighbors’ method described above.

ACKNOWLEDGEMENTS

The work of G.A., F.D. and M.G. was partially supported by NEIU Research Communities grants. The work of M.G was partially supported by NSF grant: DMS 0601016.

REFERENCES

1. E.A. BELBRUNO AND B. MARSDEN, *Resonance hopping in comets*, The Astronomical Journal 113 (1997), pp. 1433-1444.
2. G. CONTOPOULOS AND N. VOGLIS, *A fast method for distinguishing between order and chaotic orbits*, Astron. Astrophys. 317 (1997), pp. 73-81.
3. C. FROESCHLÉ AND E. LEGA, *Twist angles: a method for distinguishing islands, tori and weak chaotic orbits. Comparison with other methods of analysis*, Astron. Astrophys. 334 (1998), pp. 355-362.
4. M.J. HOLMAN AND P.A. WIEGERT, *Long-term Stability of Planets in Binary Systems*, Astron. J. 117 (1999), pp. 621-628.
5. M. GIDEA AND M. BURGOS, *Chaotic transfers in three- and four-body systems*, Physica A 328 (2003), pp. 360-366.
6. M. GIDEA AND F. DEPPE, *Chaotic Orbits in a Restricted Three-Body Problem: Numerical Experiments and Heuristics*, Communication in Nonlinear Science and Numerical Simulation, 11 (2006), pp. 161-171.
7. M. GIDEA AND J. MASDEMONT, *Geometry of homoclinic connections in a planar circular restricted three-body problem*, International Journal of Bifurcation and Chaos, to appear.
8. P. GRASSBERGER AND I. PROCACCIA, *Measuring the strangeness of strange attractors*, Physica D 8 (1983), pp. 189-208.
9. A.P. HATZES ET AL., *A Planetary Companion to γ Cephei A*, The Astrophysical Journal, 599 (2003), pp. 1383-1394.
10. J.P. HUKÉ, *Embedding Nonlinear Dynamical Systems: A Guide to Takens' Theorem*, Manchester Institute for Mathematical Sciences, 2006.
11. M.B. KENNEL, R. BROWN, H.D.I. ABARBANEL, *Determining embedding dimension for phase-space reconstruction using a geometrical construction*, Physical Review A 45 (1992), pp. 3403-3411.
12. J. LLIBRE, R. MARTÍNEZ AND C. SIMÓ, *Transversality of the invariant manifolds associated to the Lyapunov family of periodic orbits near L_2 in the restricted three-body problem*, J. Differential Equations 58 (1985), pp. 104-156.
13. A.C.J. LUO, *Predictions of quasi-periodic and chaotic motions in nonlinear Hamiltonian systems*, Chaos, Solitons and Fractals 28 (2006), pp. 627-649.

14. M.A. MURISON, M. LECAR, AND F.A. FRANKLIN, *Chaotic Motion in the Outer Asteroid Belt and its Relation to the Age of the Solar System*, *Astronomical Journal*, 108 (1994), pp. 2323–2329.
15. W.S. KOON, M.W. LO, J.E. MARSDEN AND S.D. ROSS, *Heteroclinic connections between periodic orbits and resonance transitions in celestial mechanics*, *Chaos* 10 (2000), pp. 427–469.
16. T. SAUER, J. YORKE, AND M. CASDAGLI, *Embedology*, *J. Stat. Phys.* 65 (1991), pp. 579–616.
17. V. SZEBEHELY, **Theory of Orbits**, Academic Press, Orlando, 1967.
18. J.C. SPROTT, **Chaos and Time-Series Analysis**, Oxford University Press, 2003.
19. F. TAKENS, *Detecting Strange Attractors in Turbulence*, in **Dynamical Systems and Turbulence**, D.A. Rand and L.-S. Young (eds.), *Lecture Notes in Mathematics*, Vol. 898, Springer Verlag, New York, 1981.
20. K. TSIGANIS, H. VARVOGLIS AND J.D. HADJIDEMETRIOU, *Stable chaos in the 12:7 mean motion resonance and its relation to the stickiness effect*, *Icarus* 146 (2000), pp. 240–252.
21. L. VELA-AREVALO AND J.E. MARSDEN, *Time-frequency analysis of the restricted three-body problem: transport and resonance transitions*, *Class. Quantum Grav.* 21 (2004), S351–S375.